ISSN 0003-701X, Applied Solar Energy, 2015, Vol. 51, No. 2, pp. 120–128. © Allerton Press, Inc., 2015.

HELIOTECHNICAL MATERIALS SCIENCE

Fabrication of Dye Sensitized Solar Cells with Different Anchoring Mode Based Triphenylamine Dyes[1]

Gachumale Saritha Reddy and Sambandam Anandan*

Nanomaterials and Solar Energy Conversion Lab, Department of Chemistry, National Institute of Technology, Tiruchirappalli, India

**e-mail: sanand@nitt.edu*

Received October 21, 2014

Abstract—Two new organic sensitizers of type D-π-A (Donor-π-Acceptor) and D-(π-A)$_2$ were designed and synthesized to understand the effect of anchoring mode towards TiO_2 film which leads to influence the efficiency of the fabricated dye sensitized solar cells. These dyes were synthesized based on the triphenylamine as electron donor, phenylhydrazine as π-conjugated spacer and 4-iodobenzoic acid as anchoring/acceptor group and characterized by ^1H, ^{13}C NMR and mass spectroscopy studies. The optical absorption of sensitizers shows red shift as well as high molar extinction co-efficient with extension of the π-conjugation and the quantum chemical calculation studies were performed to provide sufficient driving force for electron injection into conduction band of TiO_2. The DSSC based on type D-(π-A)$_2$ shows power conversion efficiency (PCE = η) 1.07% under simulated AM 1.5 G; due to more positive HOMO values, higher IPCE values, high adsorption capacity on TiO_2 as well as longer electron life time of dye.

DOI: 10.3103/S0003701X15020139

INTRODUCTION

After Gratzel solar cells [1], dye-sensitized solar cells (DSSC) shows more attention on both academic as well as industrial communities due to high efficiency at low cost [2, 3]. Based on above consideration, for the purpose of decrease fabrication cost and for increase power conversion efficiency (PCE) most research activities currently focusing on the metal free organic sensitizers [4] because they offer better advantages over other sensitizers, which include higher molar absorption coefficients through intramolecular π–π* transitions and can be designed more easily and economically, high purity and environment friendly [3, 5, 6] and convenient spectral modifications [4, 7] have shown the PCE (η) > 10% [8], when compared with the conventional ruthenium based chromophores (for example ruthenium-based sensitizers with conversion efficiencies beyond 12.3% [9, 10]).

The basic stratagem involved in the metal free organic dyes are Donor-π-Acceptor (D-π-A) configuration, based on this construction variety of organic dyes such as carbazole [11, 12], coumarin [13–15], indoline [16, 17], triphenylamine [18, 19], squaraine [20, 21], phenothiazine [22, 23] have been used for fabrication of DSSC. However, D-π-A rod like configuration facilitates lower PCE is due to dye aggregation at the semiconductor surface [24–26] and the recombination of conduction band electrons with triiodide in the electrolyte [27]. To avoid these problems, several dianchoring organic dyes have been proposed to increase the optical density and binding strength of dyes onto titania by involving two anchoring groups in one molecule which may abate dye aggregation as well as charge recombination; and as a result an improved photoresponse, photocurrent, and stability [28–30] due to extension of π-conjugation. Among these organic dyes, triphenylamine (TPA)-based organic dyes shows promising performances in DSSC application because of the non planar structure of TPA suppresses the dye aggregation as well as charge recombination and these dyes shows PCE up to 10% [31, 32].

Based on the above concept, herein designed and synthesized two new organic dyes (i) monoanchoring ((E)-4-(2-(4-(diphenylamino)benzylidene)-1-phenylhydrazinyl)benzoic acid (MIBA)) and (ii) bianchoring (4,4'-(2E,2'E)-2,2'-(4,4'-(phenylazanediyl)bis(4,1-phenylene)bis(methan-1-yl-1-ylidene)) bis (1-phenylhydrazin-1-yl-2-ylidene) dibenzoic acid (BIBA)) (see Scheme) and compared these dyes towards fabrication of DSSC. In this dyes, the non planar structure of TPA can act as a donor moiety, phenylhydrazine act as a π-conjugation spacer and 4-iodobenzoic acid act as a anchoring/acceptor group. The synthesized dyes were well characterized by ^1H, ^{13}C NMR and mass spectroscopic analysis (see supporting information); and in addition their spectral and redox properties were studied through experimental and theoretical approach. Further, comparison studies were performed such as the electrooptical and photovoltaic performance for both dianchoring organic dye (BIBA) and monoanchoring organic dye (MIBA).

[1] The article is published in the original.

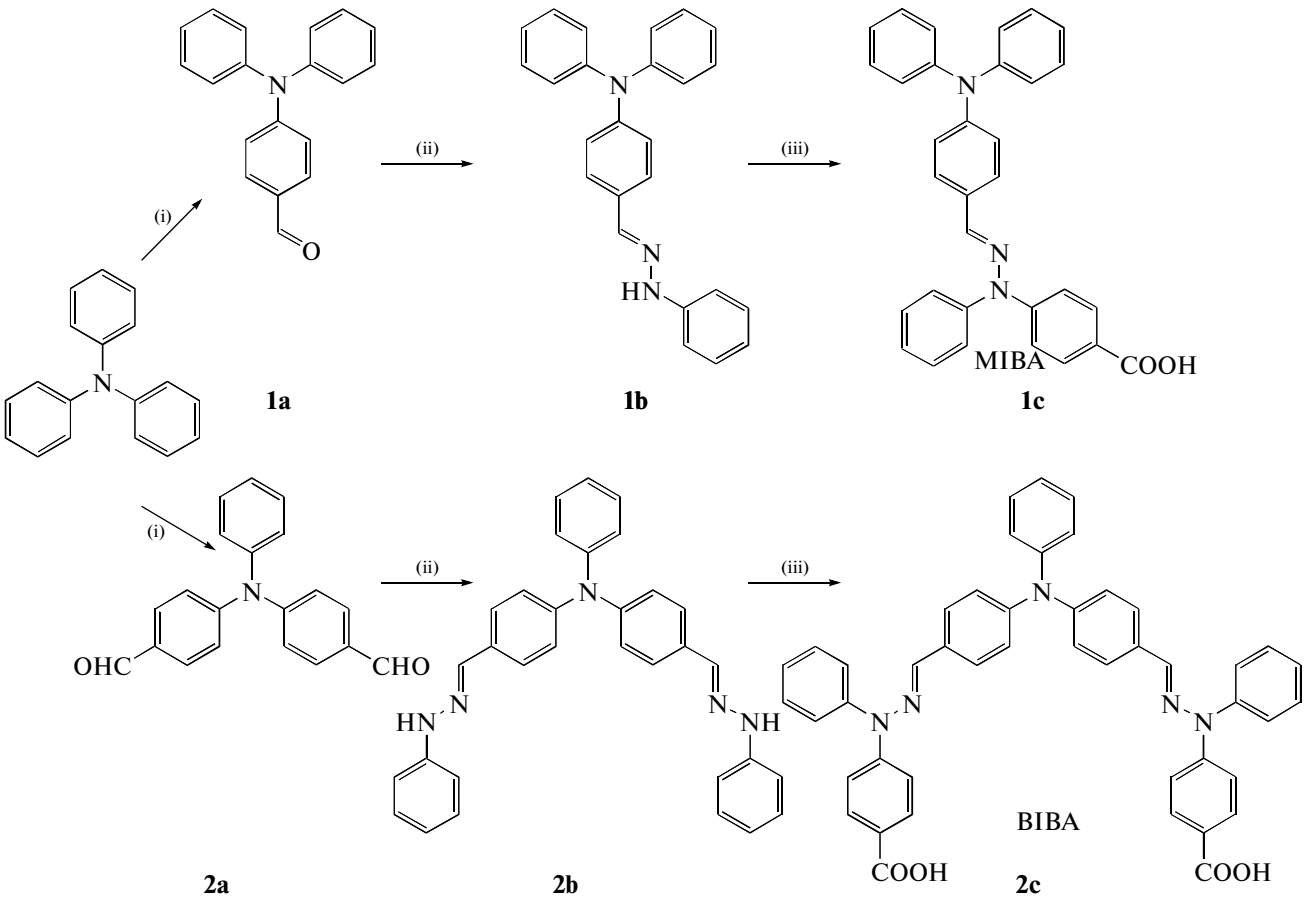

Scheme. Synthetic pathway of the organic dyes. 1: (i) $POCl_3$ (21 eq), DMF (25 eq). (ii) Phenylhydrazine (2 eq), Methanol (15 vol). (iii) CuI (0.05 eq), K_2CO_3 (2 eq), 4-iodo benzoic acid (1 eq), 1,10-phenanthralene (0.1 eq), DMF (30 vol). 2: (i) $POCl_3$ (25 eq), DMF (23 eq). (ii) Phenylhydrazine (4 eq), Methanol (30 vol). (iii) CuI (0.1 eq), K_2CO_3 (4 eq), 4-iodo benzoic acid (2 eq), 1,10-phenanthralene (0.2 eq), DMF (30 vol).

2. EXPERIMENTAL SECTION

2.1. Materials

All reagents and chemicals were purchased from Alfa Aesar and Sigma-Aldrich and used without further purification unless specified otherwise. All solvents were dried by refluxing for at least 24 h over CaH_2 and freshly distilled prior to use. All column chromatographic separations were carried out on Merck silica gel (60–120 mesh). FTO glass plates (sheet resistance 10 Ohm/□) were purchased from BHEL, INDIA.

2.2. Synthesis

2.2.1. Synthesis of 4-formyltriphenylamine (1a). Compound **1a** was prepared according to the reported literature [33]. Freshly distilled $POCl_3$ (21 eq) was added drop wise to DMF (25 eq) under an atmosphere of N_2 at 0°C, and then it was stirred for 1 h. TPA (2 g, 8.16 mmol) was added to the above solution, and the resulting mixture was stirred for 18 h at 95°C. After cooling to room temperature, the mixture was poured into a beaker containing ice-cube, and basified with 6 M NaOH. Filtered the solid and extracted with ethylacetate (EA)/brine. After evaporating the organic solvent the crude product was purified by column chromatography on silica using hexane, to give a pale yellow solid (Yield: 84%; 1.89 g).

^{1}H NMR ($CDCl_3$, ppm): δ 9.80 (s, 1H), 7.68–7.66 (m, 2H), 7.35–7.32 (m, 4H), 7.16 (t, 6H, J = 7.2 Hz), 7.01 (d, 2H, J = 8.4 Hz). ^{13}C NMR ($CDCl_3$, ppm): δ 190.48, 152.03, 145.53, 131.34, 131.31, 130.16, 127.08, 126.27, 122.78.

2.2.2. Synthesis of (E)-N,N-diphenyl-4-((2-phenylhydrazono)methyl)aniline (1b). Compound **1b** was prepared according to the reported literature [34]. The compound 1a (1 g, 3.65 mmol) was added to 100 mL single neck round bottom flask containing 15 mL freshly distilled methanol, and then stirred for 2 h at 65°C. Phenylhydrazine (2 eq) was added to the above

reaction mixture after that the reaction mixture was refluxed for 2 h. It was monitored by TLC. Filter the yellow color solid compound by using methanol as washing solvent. It was recrystallized in dichloromethane to give the product (Yield: 95%; 1.14 g).

^{1}H NMR (DMSO-d_6, ppm): δ 10.22 (s, 1H), 7.81 (s, 1H), 7.53 (d, 2H, J = 8.8 Hz), 7.30 (t, 4H, J = 8.0 Hz), 7.20–7.16 (m, 2H), 7.07–7.01 (m, 8H), 6.95 (d, 2H, J = 8.8 Hz), 6.70 (t, 1H, J = 7.2 Hz). ^{13}C NMR (DMSO-d_6, ppm): δ 146.96, 146.91, 145.38, 136.23, 130.04, 129.53, 129.03, 126.74, 124.10, 123.22, 122.94, 118.42, 111.81.

2.2.3. Synthesis of (E)-4-(2-(4-(diphenylamino)benzylidene)-1-phenylhydrazinyl)benzoic acid (1c). Compound **1c** was prepared according to the reported literature [35]. The compound 1b (0.5 g, 1.37 mmol), CuI (0.05 eq), K_2CO_3 (2 eq), 1,10-phenanthralene (0.1 eq), 4-iodobenzoic acid (1 eq) were added to the freshly distilled DMF (15 mL) under an atmosphere of N_2 at room temperature (RT), and then it was stirred for 24 h at 120°C. It was monitored by TLC. A red color solid was formed. After cooling to room temperature, the mixture was poured into a beaker containing ice-cube and then extracted with ethylacetate (EA)/brine. After evaporating the organic solvent the crude product was purified by column chromatography on silica using a mixture of EA/Hexane (1 : 6, v/v), to give a grayish yellow solid (Yield: 55%; 0.36 g).

^{1}H NMR (DMSO-d_6, ppm): δ 7.88 (d, 1H, J = 8.4 Hz), 7.77–7.73 (m, 1H), 7.65–7.60 (m, 5H), 7.45–7.37 (m, 7H), 7.29–7.09 (m, 8H), 6.99 (d, 2H, J = 8.0 Hz). ^{13}C NMR (DMSO-d_6, ppm): δ 147.86, 146.70, 146.10, 138.51, 137.36, 131.17, 130.74, 129.99, 129.83, 129.60, 129.01, 128.79, 127.69, 126.36, 125.69, 124.95, 124.66, 124.45, 123.58, 122.22, 113.99. ESI-MS Anal. Calcd. for $C_{32}H_{25}N_3O_2$: 483.56. Found: 482.

2.2.4. Synthesis of 4,4'-Diformaltriphenylamine (2a). Compound **2a** was prepared according to the reported literature [33, 36]. Freshly distilled $POCl_3$ (25 eq) was added drop wise to DMF (23 eq) under an atmosphere of N_2 at 0°C, and then it was stirred for 1 h. TPA (2 g, 8.16 mmol) was added to the above solution, and the resulting mixture was stirred for 4 h at 95°C. After cooling to room temperature, the mixture was poured into a beaker containing ice-cube, and basified with 4 M NaOH. Filtered the solid and extracted with ethylacetate (EA)/brine. After evaporating the organic solvent the crude product was purified by column chromatography on silica using a mixture of EA/Hexane (1 : 6, v/v), to give a yellow solid (Yield: 59%; 1.45 g).

^{1}H NMR (DMSO-d_6, ppm): δ 9.86 (s, 2H), 7.82 (d, 4H, J = 8.8 Hz), 7.47–7.43 (m, 2H), 7.31–7.27 (m, 1H), 7.19 (d, 3H, J = 7.6 Hz), 7.15 (d, 3H, J = 8.4 Hz). ^{13}C NMR (DMSO-d_6, ppm): δ 191.09, 151.37, 145.04, 131.24, 130.93, 130.30, 127.02, 126.29, 122.39.

2.2.5. Synthesis of N-phenyl-4-((E)-(2-phenylhydrazono)methyl)-N-(4-((E)-(2-phenylhydrazono) methyl) phenyl) aniline (2b). The compound **2a** (1 g, 3.31 mmol) was added to 100 mL single neck round bottom flask containing 15 mL freshly distilled methanol, and then stirred for 30 min at 65°C. Phenylhydrazine (4 eq) was added to the above reaction mixture after that the reaction mixture was refluxed for 1 h. It was monitored by TLC. Filter the yellow color solid compound by using methanol as washing solvent. It was recrystallized in dichloromethane to give the product (Yield: 73.3%; 1.17 g).

^{1}H NMR (DMSO-d_6, ppm): δ 10.24 (s, 2H), 7.82 (s, 2H), 7.56 (d, 4H, J = 8.8 Hz), 7.35–7.31 (m, 2H), 7.21–7.15 (m, 4H), 7.10–6.99 (m, 11H), 6.71 (t, 2H, J = 7.2 Hz). ^{13}C NMR (DMSO-d_6, ppm): δ 146.62, 146.59, 145.35, 136.16, 130.44, 129.62, 129.04, 126.79, 124.43, 123.58, 123.44, 118.46, 111.83.

2.2.6. Synthesis of 4,4'-(2E,2'E)-2,2'-(4,4'-(phenylazanediyl)bis(4,1-phenylene)bis(methan-1-yl-1-ylidene)) bis(1-phenylhydrazin-1-yl-2-ylidene)dibenzoic acid (2c). The compound **2b** (0.5 g, 1.03 mmol), CuI (0.1 eq), K_2CO_3 (4 eq), 1,10-phenanthralene (0.2 eq), 4-iodobenzoic acid (2.5 eq) were added to the freshly distilled DMF (15 mL) under an atmosphere of N_2 at RT, and then it was stirred for 24 h at 120°C. It was monitored by TLC. A red color solid was formed. After cooling to room temperature, the mixture was poured into a beaker containing ice-cube and then extracted with ethylacetate (EA)/brine. After evaporating the organic solvent the crude product was purified by column chromatography on silica using a mixture of EA/Hexane (1 : 6, v/v), to give a grayish yellow solid (Yield: 45%; 0.20 g).

^{1}H NMR ($CDCl_3$, ppm): δ 7.89 (d, 4H, J = 8.8 Hz), 7.55 (t, 4H, J = 7.6 Hz), 7.46–7.41 (m, 6H), 7.18 (t, 7H, J = 7.6 Hz), 7.09–6.97 (m, 12H). ^{13}C NMR ($CDCl_3$, ppm): δ 150.44, 130.59, 130.01, 128.86, 128.75, 128.48, 126.68, 124.39, 122.51, 112.97. ESI-MS Anal. Calcd. for $C_{46}H_{35}N_5O_4$: 721.80. Found: 722.

2.3. Preparation of Dye-Sensitized TiO_2 Thin Films

The photoanode was prepared by the following procedure as follows [37]: The glacial acetic acid (5 mL), 7.5 mL of tetra isopropyl titanate ($C_{12}H_{28}O_4Ti$) and one drop of Triton X-100 were mixed with 15 mL of 2-propanol. Water (5 mL) was added to the above solution drop wise while vigorously stirring the solution. The resulting semi colloidal suspension was dispersed on fluorine doped tin oxide (FTO) glass plate by using doctor blade technique. Loose crust on TiO_2 film was removed by wiping smoothly using cotton wool. The thickness of the TiO_2 film (12 μm) was successively controlled, by repeating

the above coating procedure. Then it was sintered at 450°C for 1 h for removing the binder, solvent and giving an electrically-connected network of TiO_2 particles under tubular furnace. After the sintering process, when the temperature of the plate drops to 50 to 70°C, it was immersed into the dye solution and kept at 25°C for 24 h so that the dye could be adsorbed onto the surface of the TiO_2 electrodes. Excess non-adsorbed dye was washed with anhydrous ethanol.

2.4. Dye-Sensitized Solar Cell Fabrication

The dye-deposited film is used as a working electrode. The Platinum catalyst counter electrode was prepared by deposition of $H_2PtCl_6 \cdot 6H_2O$ solution (0.005 mol dm^{-3} in isopropanol) onto FTO glass and then sintering at 400°C for 20 min was act as photocathode [38, 39]. The DSSC device was fabricated by the following method: the photo cathode was placed on top of the photo anode and was tightly clipped together. Then, liquid electrolyte 0.05 M I_2/0.5 M LiI/0.5 M 4-*tert*-butyl pyridine (TBP) in 3-methoxypropionitrile was injected in-between the two electrodes.

2.5. Characterization of the Dyes

^1H and ^{13}C NMR spectra were realized on a 400/600 MHz BRUKER spectrometer in deuterated chloroform or dimethylsulfoxide solution at 298 K. Chemical shifts (δ values) were recorded in units of ppm relative to tetramethylsilane (TMS) as an internal standard. The molecular weights of the dyes were determined by Micromass QUATTRO 11 ESI-MS spectrometer coupled to a Hewlett Packard series 1100 degasser. Absorption and fluorescence spectra were measured in DMF solution on a Specord S 600 diode-array UV-vis spectrophotometer and Shimadzu RF-5301 PC spectrofluorophotometer respectively. Electrochemical measurements were performed on a Metrohm Autolab PGSTAT potentiostat/galvanostat-84610. All measurements were carried out at room temperature with a conventional three-electrode configuration consisting of a platinum disc working electrode, a glassy carbon (GC) auxiliary electrode, and an Ag/AgCl (aq) was used as the reference electrode. The potentials were reported vs. ferrocene as standard using a scan rate of 0.1 V s^{-1} and the sample solutions contained 3×10^{-4} M sample and 0.1 M tetrabutylammonium hexafluorophosphate (TBAHFP) in anhydrous DMF as a supporting electrolyte under Argon atmosphere. Electrochemical impedance spectroscopy (EIS) measurements were done under 85 mW cm^{-2} light illumination by using an Autolab PGSTAT potentiostat/galvanostat-84610. The impedance spectra were recorded with a frequency ranging between 10 kHz to 1 Hz at their open circuit potential (OCP). The IPCE spectra were recorded using Oriel 300W Xe Arc lamp in combination with an Oriel Cornerstone $260^{1/4}$ monochromator. The number of incident photons was calculated for each wavelength using a calibrated monocrystalline silicon diode as reference.

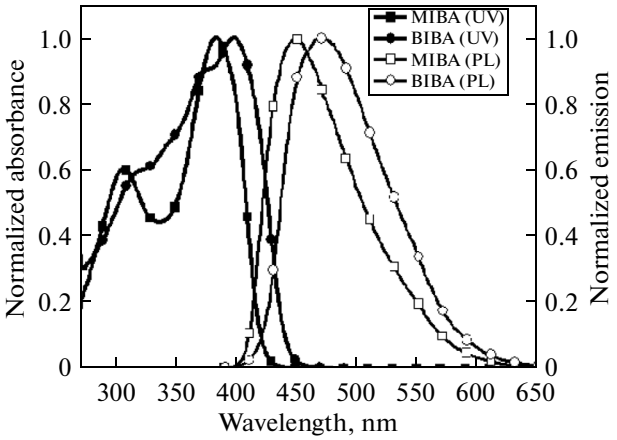

Fig. 1. Normalized UV-vis absorption and fluorescence emission spectra of synthesized dyes recorded in DMF (6×10^{-5} M) solution.

3. RESULTS AND DISCUSSION

3.1. Synthesis of Organic Dyes

Scheme shows the synthetic pathways of organic dyes MIBA and BIBA. The Vilsmeier-Haack formylation of triphenylamine gave aldehyde compounds 4-formyltriphenylamine (**1a**) and 4,4'-Diformaltriphenylamine (**2a**) respectively. The synthesized aldehydes (**1a** and **2a**) were involved in condensation reaction with phenylhydrazine to yield hydrazones (**1b**) and (**2b**). It is then arylated with 4-iodobenzoic acid to obtain the product (**1c**) and (**2c**). All the intermediates and target products were purified by column chromatography and the new compounds were well confirmed by various analytical tools (See Supporting information).

3.2. Optical Properties

Figure 1 shows the absorption and emission spectra of the synthesized organic dyes (MIBA and BIBA) in DMF (6×10^{-5} M) solution and the corresponding data were summarized in Table 1.

As can be seen in Fig. 1, both MIBA and BIBA compounds exhibit two major prominent bands, one was appearing in range of 300–320 nm and another one in the range of 380–400 nm, respectively. The former is ascribed to a localized aromatic π–π* transition of the conjugated aromatic rings and the later is of intramolecular charge transfer (ICT) between the triphenylamine donating unit and 4-iodobenzoic acid acceptor/anchoring moiety, thereby producing an efficient charge separated state [40]. However, the absorption of the dianchoring organic dye BIBA (399 nm) in the conjugation pathway is red-shifted by

Table 1. Summary of electrooptical parameters of the dyes

Dye	λ_{abs}, nm (ε, M^{-1} cm^{-1})[a]	λ_{em}, nm[a, b]	E_g^{opt}, (eV)[c]	E_{ox}, V (vs. Fc)	E_{HOMO}, (eV)[d]	E_{LUMO}, (eV)[d]	HOMO[e]	LUMO[e]
MIBA	308 (22304), 384 (36924)	448	3.0	0.82	5.17	2.17	−4.93	−1.39
BIBA	317 (29805), 399 (45969)	469	2.87	0.87	5.22	2.35	−4.82	−1.74

[a] Absorption and emission spectra were recorded in DMF solution (6×10^{-5} M) at room temperature. [b] Dyes were excited at their absorption maximum value (for MIBA, $\lambda_{ex} = 405$ nm and for BIBA, $\lambda_{ex} = 411$ nm). [c] Optical band gap calculated from intersection between the absorption and emission spectra. [d] The values of E_{HOMO} and E_{LUMO} were calculated with the following: HOMO (eV) = $-e(E_{onset}^{ox}$, V (vs. Fc/Fc^+) + 4.8 V); LUMO (eV) = $E_{onset}^{ox} - E_{0-0}$, where E_{0-0} is the intersection between the absorption and emission spectra of the sensitizers. [e] B3LYP/6-31G(d,p) calculated values.

15 nm compared to MIBA (384 nm) dye. This is because the increase of electron acceptors in dye molecule is beneficial to intramolecular charge transfer [33]. Moreover, the molar extinction coefficients (ε) of BIBA ($\varepsilon = 45.969$ M^{-1} cm^{-1}) is larger than MIBA ($\varepsilon =$ 36.924 M^{-1} cm^{-1}) dye. Dyes MIBA and BIBA exhibit high extinction coefficients (Table 1), for example, the value of ε for BIBA ($\varepsilon = 4.5 \times 10^4$ M^{-1} cm^{-1} at 399 nm) is more than three times higher than that of the standard Z907 ruthenium sensitizer ($\varepsilon = 1.2 \times 10^4$ M^{-1} cm^{-1} at 521 nm) [41]. The higher molar extinction coefficient value of BIBA dye enhances electrolyte diffusion in the film and reduces the recombination of the light induced charges during transportation [42], which might have increases the photocurrent, photo voltage and overall positive effect on the device performance. The fluorescence spectra recorded upon their excitation of absorption maxima value of MIBA and BIBA exhibit luminescence maxima at 448 nm ($\lambda_{ex} = 405$ nm) and 469 nm ($\lambda_{ex} = 411$ nm) respectively.

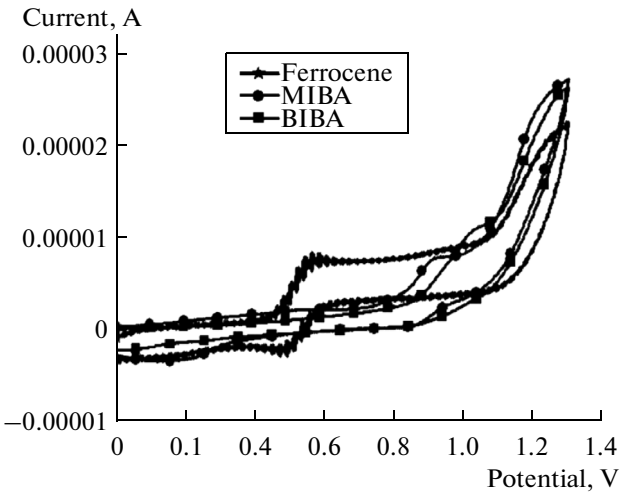

Fig. 2. Cyclic voltammograms of dyes were measured in DMF solution with Bu_4NPF_6 (0.1 M) as an electrolyte. Working electrode: Pt; reference electrode: Ag/AgCl(aq); counter electrode: Glassy carbon; calibrated with Fc/Fc^+ as a standard reference; scan rate: 0.1 V s^{-1}.

3.3. Electrochemical Properties

Cyclic voltammetry was performed to estimate the onset oxidation potentials (E_{onset}^{ox}) of the synthesized dyes, which are corresponding to HOMO energy levels of dyes. The E_{onset}^{ox} are observed at 0.82 V (MIBA) and 0.87 V (BIBA) were determined from the intersection of two tangents drawn at the rising current and background charging current of a cyclic voltammograms [43] in DMF medium (Fig. 2) and the corresponding data were shown in Table 1.

The HOMO and LUMO level of the dyes shown in Fig. 3. The HOMO energy levels were calculated based on the relationship of HOMO (eV) = $-e$ (E_{onset}^{ox}, V (vs. Fc/Fc^+) + 4.8 V) by assuming the ferrocene (Fc) energy level to be −4.8 eV below the vacuum level [44]. The observed HOMO values are more positive than I^-/I_3^- redox couple (−4.6 eV vs. vacuum) ensuring the thermodynamic regeneration of the dyes. LUMO levels of these dyes were sufficiently more negative than the conduction band energy level (E_{cb}) of TiO_2, which implies that electron injection from the excited dye into conduction band of TiO_2 is feasible [45], and these LUMO energy values are calculated by (E_{onset}^{ox}) − E_{0-0}, where E_{0-0} is the zero-zero energy of the dyes estimated from the intersection between absorption and emission spectra [46]. The HOMO level of BIBA

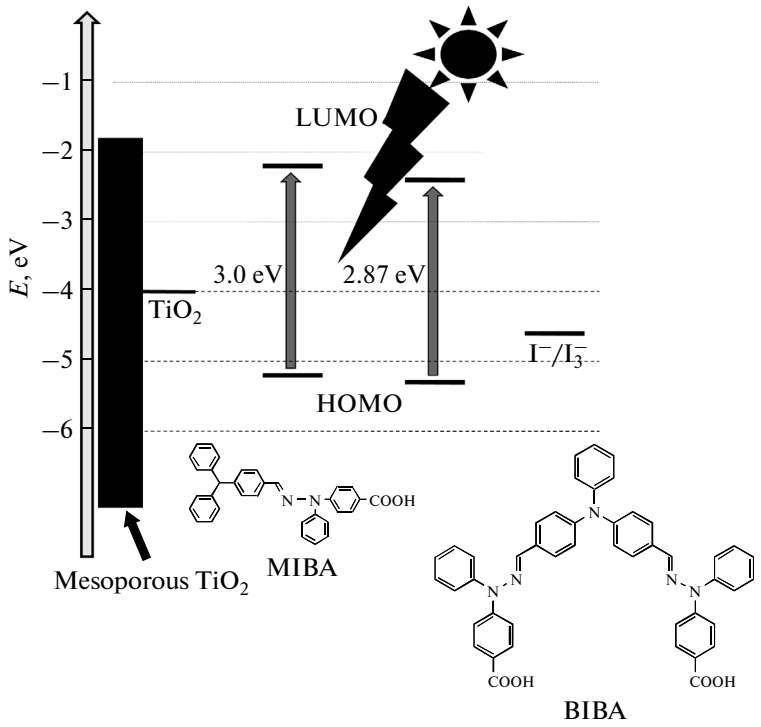

Fig. 3. The pictorial representation of experimental HOMO and LUMO energy levels of the synthesized sensitizers.

more positive than that of MIBA dye, which may increase the power conversion efficiency [47].

3.4. Theoretical Calculation

Density functional theory (DFT) calculations using B3LYP/6-31G(d,p) level in gas phase with Gaussian 09 program was performed to get study on the molecular geometries and electron distribution of the synthesized organic dyes with optimized structures. As can be seen in Fig. 4, the electron density mainly dominated on the donor moiety triphenylamine and π-bridge phenylhydrazine at the HOMO level, whereas at the LUMO level the electron density is mainly located on the π-bridge as well as anchoring/acceptor moiety 4-iodobenzoicacid for both dyes, which is due to intra molecular charge transfer along the π-conjugated skeleton. The calculated HOMO and LUMO energies of the dyes were listed in Table 1. Therefore, the spatial separation of HOMO and LUMO energy levels of the dyes is suitable for DSSC, which indicates that an efficient photo induced electron transfer from dye to the conduction band of TiO_2. Generally, the twisted non-planar geometric structure of triphenylamine unit can reduce contact between molecules, effectively suppress the charge recombination, enhance their open-circuit voltage and it will effect on overall device performance.

3.5. Photovoltaic Performance of the DSSC

As presented in Fig. 5, the current density-voltage (J–V) characteristics of DSSC sensitized with MIBA and BIBA are recorded under simulated AM 1.5 G illumination (85 mW cm^{-2}) and the detailed parameters are shown in Table 2. The DSSC based on BIBA cell exhibited a PCE (η) of 1.07%, which is superior compared to the cell sensitized with MIBA (η = 0.57%) under same conditions.

	MIBA	BIBA
OPTIMIZED STRUCTURE	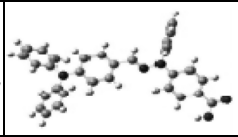	
HOMO		
LUMO		

Fig. 4. The frontier molecular orbital's of the HOMO and LUMO levels of synthesized dyes calculated at B3LYP/6-31G(d, p) with optimized structure.

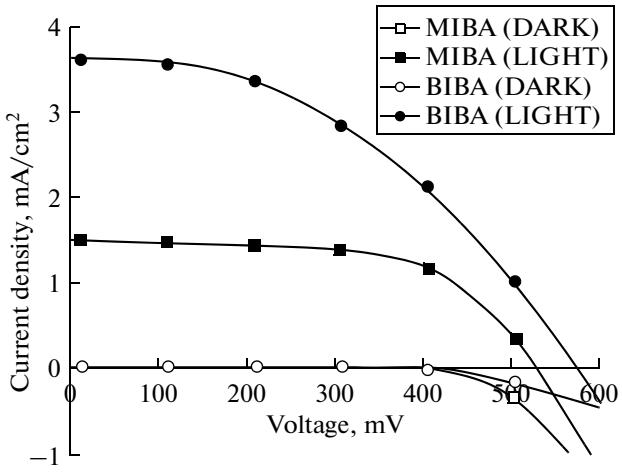

Fig. 5. Current density-voltage characteristics for MIBA and BIBA based devices for DSSC under illumination of simulated solar light (AM 1.5 G, 85 mW cm^{-2}).

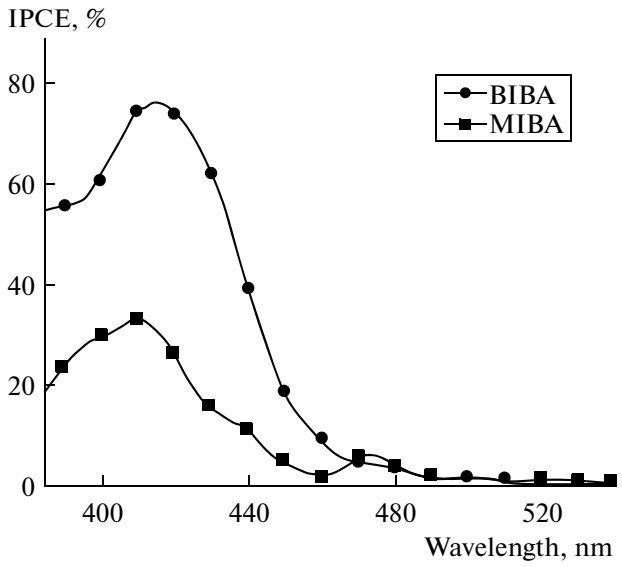

Fig. 6. The incident photon-to-current conversion efficiency of DSSC based on the synthesized organic dyes MIBA and BIBA.

It is attributed to the relatively higher short circuit current density (J_{sc}), open circuit photo voltage (V_{oc}). Mainly higher J_{sc} stem from its absorption red shift, high molar extinction coefficient in the visible region [48] and its lowered HOMO level of BIBA compared to MIBA allows efficient regeneration of the oxidized dye and as well as minimize the charge recombination. High J_{sc} values indicate high electron collection efficiencies which in turn indicate faster electron diffusion rates [49].

The incident photon-to-current conversion efficiency (IPCE) for the DSSC based on dyes MIBA and BIBA are shown in Fig. 6. The IPCE values of both MIBA and BIBA sensitized cells are observed at 409, 415 nm and exhibited 33.8, 76% respectively. The IPCE spectrum of BIBA is red shifted compared to that of MIBA dye as a result of extra branching unit, and in addition the increase of dye adsorbed amount led to action spectrum broadening and the IPCE value increasing [50]. The IPCE maxima increased in order with J_{sc}, the higher IPCE and J_{sc} could lead to an improved photovoltaic performance of the DSSC based on dye BIBA. In addition to this, the increase in value of V_{oc} attributed by the increased life time of DSSC based on BIBA [51] (Fig. 7b). This is further confirmed by calculating the adsorbed amounts (Γ) of dyes on TiO_2 surface by desorption of the dye from the TiO_2 surface using 0.1 M NaOH in DMF/H_2O (1 : 1) mixture [52]. BIBA adsorbs comparatively more on TiO_2 surface than that of MIBA dye, which may further augment the device performance.

3.6. Electrochemical Impedance Spectroscopy (EIS)

Electrochemical impedance spectroscopy analysis [53, 54] was performed to study interfacial charge transfer processes in DSSCs based on MIBA and BIBA dyes and they were measured over a frequency range of 10^0–10^4 Hz under AM 1.5. As shown in Figs. 7a and 7b, Nyquist and Bode phase plots typically have two semicircles and two frequency peaks for both MIBA and BIBA dyes, respectively. Usually, the smaller semicircle corresponds to the high-frequency peaks of Bode plots, which represents mainly the electron transfer process from the Pt counter electrode to the oxidized species in the electrolyte. The larger semicircle corresponding to the low frequency peaks of Bode plots is ascribed to the recombination resistance across the TiO_2/redox electrolyte interface [55]. The radius of the larger semicircle in the order of BIBA < MIBA indicating the electron transport is

Table 2. Photovoltaic parameters of DSSCs based on the synthesized dyes

Dye	J_{sc}, mA cm^{-2}	V_{oc}, mV	FF	η, (%)[a]	IPCE, %	Surface concentration Γ, mol/cm^2	Electron lifetime (τ_{eff}), ms
MIBA	1.49	526	0.62	0.57	33.8	5.2×10^{-6}	37.11
BIBA	3.59	579	0.43	1.07	76	5.8×10^{-6}	46.99

[a] Illumination: 85 mW cm^{-2} simulated AM 1.5 G solar light; electrolyte containing: 0.05 M I_2/0.5 M LiI/0.5 M 4-*tert*-butyl pyridine in 3-methoxypropionitrile.

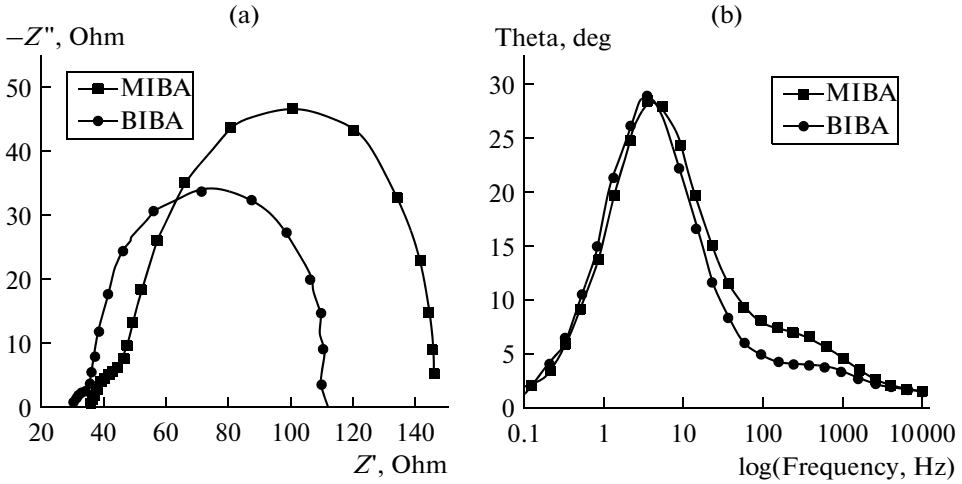

Fig. 7. Electrochemical impedance spectra of DSSCs under illumination of simulated solar light (AM 1.5 G, 85 mW cm^{-2}). (a) Nyquist plots. (b) Bode phase plots.

decreases in the order of BIBA < MIBA which reflected in the efficiency of devices [56].

From Bode phase plot (Fig. 7b), the electron lifetime (E_{eff}) for the cells of MIBA (37.11 ms) and BIBA (46.99 ms) were calculated by using the following equation [57]: $\tau_{eff} = 1/2\pi f$, where f is the frequency peak in Bode phase plot. Longer electron lifetime indicate improved suppression of the back reaction between the injected electrons and the electrolyte; they lead to improvement of V_{oc} due to reduced charge recombination rate [58], reflecting in the improvement of the photocurrent and yielding substantially enhanced overall conversion efficiency.

4. CONCLUSIONS

Based on anchoring mode, designed and synthesized here two metal free organic dyes (MIBA and BIBA) with triphenylamine as electron donor, phenylhydrazine as π-conjugated spacer and 4-iodobenzoic acid as electron acceptor/anchoring group. The effect of anchoring mode on optical, electrochemical and photovoltaic properties were studied and developed for DSSC. Upon fabricated devices, the BIBA dye exhibit highest efficiency due to the high molar extinction coefficient value with extension of π-conjugation, the more positive HOMO level value, longer electron life time on the TiO_2 semiconductor surface as well as the more IPCE values may enhance the power conversion efficiency than the monoanchoring MIBA dye, which means that the dianchoring mode is more suitable for further device fabrication studies.

Supplementary Material

Spectral data and Cartesian Coordinates of the Optimized organic dyes at the B3LYP/6-31G (d,p) level of theory.

ACKNOWLEDGMENTS

Author SA thank SERI-DST, New Delhi (no. DST/TM/SERI/2k12/109(C)) and DST-FIST, New Delhi (SR/FT/CSI-190/2008 dated 16th Mar 2008) for the sanction of research fund towards development of new facilities. Author GSR thanks MHRD, New Delhi for the junior research fellowship position.

REFERENCES

1. Regan, B.O. and Gratzel, M., *Nature*, 1991, vol. 353, pp. 737–740.
2. Gratzel, M., *Acc. Chem. Res.*, 2009, vol. 42, pp. 1788–1798.
3. Hagfeldt, A., Boschloo, G., Sun, L.C., et al., *Chem. Rev.*, 2010, vol. 110, pp. 6595–6663.
4. Mishra, A., Fischer, M., and Bäuerle, P., *Angew. Chem., Int. Ed.*, 2009, vol. 48, pp. 2474–2499.
5. Tian, H. and Meng, F., *Organic Photovoltaics: Mechanisms, Materials, and Devices*, Sun, S.-S. and Sariciftci, N.S., London: CRC, 2005.
6. Karki, I.B., Nakarmi, J.J., Mandal, P.K., et al., *Appl. Solar Energy*, 2013, vol. 49, pp. 40–45.
7. Ooyama, Y. and Harima, Y., *Eur. J. Org. Chem.*, 2009, pp. 2903–2934.
8. Jiang, K.J., Xia, J.B., Masaki, N., et al., *Inorg. Chim. Acta*, 2008, vol. 361, pp. 783–785.
9. Zeng, W., Cao, Y., Bai, Y., et al., *Chem. Mater.*, 2010, vol. 22, pp. 1915–1925.
10. Yella, A., Lee, H.W., Tsao, H.N., et al., *Science*, 2011, vol. 334, pp. 629–633.
11. Hara, K., Wang, Z.S., Cui, Y., et al., *Environ. Sci.*, 2009, vol. 2, no. 10, pp. 1109–1114.
12. Lai, H., Hong, J., Liu, P., et al., *RSC. Adv.*, 2012, vol. 2, no. 6, pp. 2427–2432.
13. Agrawal, S., Dev, P., English, N.J., et al., *J. Mater. Chem.,* 2011, vol. 21, no. 30, pp. 11101–11108.

14. Hara, K., Wang, Z.S., Sato, T., et al., *J. Phys. Chem. B*, 2005, vol. 109, pp. 15476–15482.
15. Hara, K., Kurashige, M., Dan-oh, Y., et al., *New J. Chem.*, 2003, vol. 27, pp. 783–785.
16. Horiuchi, T., Miura, H., Sumioka, K., and Uchida, S., *J. Am. Chem. Soc.*, 2004, vol. 126, pp. 12218–12219.
17. Ito, S., Miura, H., Uchida, S., et al., *Chem. Commun.*, 2008, pp. 5194–5196.
18. Kitamura, T., Ikeda, M., Shigaki, K., et al., *Chem. Mater.,* 2004, vol. 16, no. 9, pp. 1806–1812.
19. Hagberg, D.P., Yum, J.H., Lee, H., et al., *J. Am. Chem. Soc.*, 2008, vol. 130, pp. 6259–6266.
20. Burke, A., Ito, S., Snaith, H., et al., *Nano. Lett.*, 2008, vol. 8, no. 4, pp. 977–981.
21. Yum, J.H., Walter, P., Huber, S., et al., *J. Am. Chem. Soc.*, 2007, vol. 129, pp. 10320–10321.
22. Marotta, G., Anil Reddy, M., Singh, S.P., et al., *ACS. Appl. Mater. Interfaces,* 2013, vol. 5, pp. 9635–9647.
23. Hart, A.S., Chandra Bikram, K.C., Subbaiyan, N.K., et al., *ACS. Appl. Mater. Interfaces*, 2012, vol. 4, pp. 5813–5820.
24. Tatay, S., Haque, S.A., Regan, B.O., et al., *J. Mater. Chem.*, 2007, vol. 17, pp. 3037–3044.
25. Ehret, A., Stuhl, L., and Spitler, M.T.J., *Phys. Chem. B*, 2001, vol. 105, pp. 9960–9965.
26. Wang, Z.S., Cui, Y., Dan-oh, Y., et al., *J. Phys. Chem. C,* 2007, vol. 111, pp. 7224–7230.
27. Liu, D., Fessenden, R.W., Hug, G.L., and Kamat, P.V.J., *Phys. Chem. B*, 1997, vol. 101, pp. 2583–2590.
28. Abbotto, A., Leandri, V., Manfredi, N., et al., *Eur. J. Org. Chem.*, 2011, pp. 6195–6205.
29. Ren, X., Jiang, S., Cha, M., et al., *Chem. Mater.*, 2012, vol. 24, pp. 3493–3499.
30. Li, Q., Shi, J., Li, H., et al., *J. Mater. Chem.*, 2012, vol. 22, pp. 6689–6696.
31. Zhang, G., Bala, H., Cheng, Y., et al., *Chem. Commun.*, 2009, no. 16, pp. 2198–2200.
32. Hwang, S., Lee, J.H., Park, C., et al., *Chem. Commun.*, 2007, pp. 4887–4889.
33. Yang, C.H., Chen, H.L., Chuang, Y.Y., et al., *J. Power Sources*, 2009, vol. 188, pp. 627–634.
34. Urnikaite, S., Malinauskas, T., Gaidelis, V., et al., *Chem. Asian J.*, 2013, vol. 3, pp. 538–541.
35. Ramkumar, S., Marutheeswaran, S., Antonius, T.M.M., and Anandan, S., *Tetrahedron Lett.*, 2011, vol. 52, pp. 3347–3352.
36. Mallegol, T., Gmouh, S., Meziane, M.A.A., et al., *Synthesis*, 2005, vol. 11, pp. 1771–1774.
37. Sirimanne, P.M. and Tributsch, H.J., *Solid State Chem.*, 2004, vol. 177, pp. 1789–1795.
38. He, J., Wu, W., Hua, J., et al., *J. Mater. Chem.*, 2011, vol. 21, pp. 6054–6062.
39. Xu, W., Peng, B., Chen, J., et al., *J. Phys. Chem. C*, 2008, vol. 112, pp. 874–880.
40. Ci, Z., Yu, X., Bao, M., et al., *Dyes Pigments*, 2013, vol. 96, pp. 619–625.
41. Cai, N., Moon, S.J., Ha, L.C., et al., *Nano. Lett.*, 2011, vol. 11, pp. 1452–1456.
42. Wu, W., Zhang, J., Yang, H., et al., *J. Mater. Chem.*, 2012, vol. 22, pp. 5382–5389.
43. Agrawal, A.K. and Jenekhe, S.A., *Chem. Mater.*, 1996, vol. 8, pp. 579–589.
44. Pomrnerehne, B.J., Vestweber, H., Gun, W., et al., *J. Adv. Mater*, 1995, vol. 7, p. 551.
45. Jones, B.A., Facchetti, A., Wasielewski, M.R., et al., *J. Am. Chem. Soc.*, 2007, vol. 129, no. 49, pp. 15259–15278.
46. Tian, H., Yang, X., Cong, J., et al., *Chem. Commun.*, 2009, no. 41, pp. 6288–6290.
47. Zhang, F., Luo, Y.H., Song, J.S., et al., *Dyes Pigments*, 2009, vol. 81, pp. 224–230.
48. Cecconi, B., Mordini, A., Reginato, G., et al., *Asian. J. Org. Chem.*, 2014, vol. 3, no. 2, pp. 140–152.
49. Maheswari, D. and Venkatachalam, P., *Appl. Solar Energy,* 2013, vol. 49, pp. 93–97.
50. Tae, E.L., Lee, S.H., Lee, J.K., et al., *J. Phys. Chem. B*, 2005, vol. 109, pp. 22513–22522.
51. Holcombe, T.W., Yum, J.H., Kim, Y., et al., *J. Mater. Chem. A*, 2013, vol. 1, pp. 13978–13983.
52. Tian, H., Yang, X., Chen, R., et al., *J. Phys. Chem. C*, 2008, vol. 112, pp. 11023–11033.
53. Kuang, D., Uchida, S., Humphry-Baker, R., et al., *Angew. Chem., Int. Ed.*, 2008, vol. 47, pp. 1923–1927.
54. Wang, Q., Moser, J.E., and Graltzel, M., *J. Phys. Chem. B,* 2005, vol. 109, pp. 14949–14953.
55. Lee, C.P., Chen, P.Y., and Vittala, R.HoK.C., *J. Mater. Chem.*, 2010, vol. 20, pp. 2356–2361.
56. Surya Prakash, S., Roy, M.S., Justin, T.K.R., et al., *J. Phys. Chem. C*, 2012, vol. 116, pp. 5941–5950.
57. Naveen Kumar, E., Jose, R., Archana, P.S., et al., *Energy. Environ. Sci*, 2012, vol. 5, pp. 5401–5407.
58. Bisquert, J., Zaban, A., Greenshtein, M., and Mora-Sero, I., *J. Am. Chem. Soc.*, 2004, vol. 126, pp. 13550–13559.